Geophysical Journal International

Geophys. J. Int. (2020) **222,** 2162–2171
Advance Access publication 2020 June 17
GJI Seismology

doi: 10.1093/gji/ggaa297

Non-stability of the noise HVSR at sites near or on topographic heights

M. La Rocca [1], G.D. Chiappetta,[1] A. Gervasi[1,2] and R.L. Festa[1]

[1]*Dipartimento di Biologia, Ecologia e Scienze della Terra, Università della Calabria, Via Pietro Bucci,* 87036 *Rende, Italy. E-mail: mario.larocca@unical.it*
[2]*Istituto Nazionale di Geofisica e Vulcanologia, Sezione ONT, Via Pietro Bucci,* 87036 *Rende, Italy*

Accepted 2020 June 12. Received 2020 June 10; in original form 2019 September 16

SUMMARY

The horizontal to vertical spectral ratio (HVSR) of seismic noise is often used to investigate site effects, and it is usually assumed to be a stable feature of the site considered. Here we show that such an assumption is not always justified, and may lead to incorrect conclusions. The HVSR analysis was performed on ambient seismic noise recordings lasting from weeks to months at many sites in Calabria, Italy. Results show a variety of site effects, from the resonance of a shallow sedimentary layer to the polarized amplification of horizontal ground motion associated with topographic effects. We describe the results of seven sites whose HVSR is characterized by dual content: one that is persistent, and another appearing only occasionally. Two sites very near the coast of the Tyrrhenian sea and five sites in the Calabrian Arc mountains show the most remarkable results. The shape of the HVSR changes significantly at these sites when the amplitude of background noise increases in a broad frequency band during periods of bad weather. The occasional contribution to the HVSR consists of one or more peaks, depending on the site, that appear only when the amplitude of ambient noise is higher than usual. The seven sites where we observe the HVSR variability are all located in complex geological environments, on mountains, ridges or foothills. A variation of the HVSR correlated with the day–night cycle is also observed at some of these sites.

Key words: Time-series analysis; Body waves; Seismic noise; Site effects; Surface waves and free oscillations; Wave propagation.

1 INTRODUCTION

The measurement of site effects has long attracted the attention of seismologists, engineers and other researchers involved in the mitigation of seismic risk. One of the simplest and most effective techniques available for this purpose is the analysis of seismic noise recorded by three-component seismometers, used to compute the spectral ratio between horizontal and vertical ground motion (HVSR). Often called the Nakamura method (Nakamura 1989, 2000), this technique is very efficient in estimating the resonance frequency in cases with soft layer on bedrock (Lermo & Chavez-Garcia 1993; Mucciarelli 1998; Mucciarelli & Gallipoli 2001; Bonnefoy-Claudet *et al.* 2006a; Borges *et al.* 2016). In such cases the layer seismic resonance is inferred from the presence of a well-defined peak in the HVSR curve, and its frequency puts a strong constraint on the layer thickness (Gueguen *et al.* 2000; Parolai *et al.* 2002; Bonnefoy-Claudet *et al.* 2006a; Gosar & Lenart 2010; Bignardi 2017). On the contrary, the same analysis applied to seismic noise recorded on flat topography with outcropping bedrock gives a rather flat HVSR. The HVSR method has been largely applied to seismic noise during the last decades to obtain a fast and cheap estimation of site effects, often for microzonation purposes (e.g. Lachet *et al.* 1996; Bour *et al.* 1998; Gueguen *et al.* 2000; Gosar & Lenart 2010; Gallipoli *et al.* 2011; Mucciarelli 2011; Strollo *et al.* 2012; Martorana *et al.* 2018, and many others). It has also been applied to earthquake recordings, and results compared with those of seismic noise recorded at the same site (Mucciarelli *et al.* 2003; Chavez-Garcia *et al.* 2018; Napolitano *et al.* 2018). The comparison has evidenced the reliability of results obtained from the seismic noise as a powerful and economic tool for the investigation of site effects (e.g. Lermo & Chavez-Garcia 1993; Bour *et al.* 1998; Mucciarelli & Gallipoli 2001; Cara *et al.* 2003; Parolai *et al.* 2010). On the other hand, many authors have shown that the amplitude of the HVSR peak can be variable and not necessarily related to the ground motion amplification observed in the case of earthquakes (Bonnefoy-Claudet *et al.* 2008; Cara *et al.* 2010; Gallipoli *et al.* 2011; Rong *et al.* 2017).

Another important site effect is that produced by the interaction of seismic waves with the topography. Ground motion amplification of the horizontal components with a polarization in the direction of the maximum slope, or normal to the ridge crest, are the most commonly observed site effects in mountain zones in the case of earthquakes (Geli *et al.* 1988; Pedersen *et al.* 1994; Bouchon & Barker 1996; Spudich *et al.* 1996; Del Gaudio *et al.* 2008;

Buech *et al.* 2010; Massa *et al.* 2010; Formisano *et al.* 2012). The dependence of ground motion amplification on the frequency of the seismic signal has also been documented. Wavelengths comparable with the size of the crest, or of the mountain, are recognized as a reliable criterion to forecast the frequency of the maximum ground motion amplification (Spudich *et al.* 1996; Paolucci 2002). Many authors have analysed earthquakes and seismic noise and compared the results to investigate the effects of the topography on the ground motion. The HVSR computed for both earthquakes and noise often show a high degree of similarity, or at least similar peaks at the same frequency (Chavez-Garcia *et al.* 1996; Parolai *et al.* 2010; Napolitano *et al.* 2018). This suggests that the simple analysis of seismic noise may be very useful for revealing at least part of the topographic effects (Chavez-Garcia *et al.* 1996; Del Gaudio *et al.* 2008; Panzera *et al.* 2011). Detailed analyses of the interaction of seismic waves with complex topography have also been performed using several methods (Chavez-Garcia *et al.* 1997; Burjanek *et al.* 2014). However, a full agreement between the results obtained from earthquakes and noise has not been observed, probably because topography effects are often superimposed on other site effects, first of all those associated with the local geological structure (Burjanek *et al.* 2014). Therefore an exhaustive comprehension of topography effects on ground motion has not yet been achieved.

One of the assumptions of the HVSR method is to treat the spectral ratio as a stable feature of the site considered. Indeed, a number of experiments have shown that the frequency of the resonance peak does not vary significantly among weak stationary noise, transient noise, traffic noise, calm or windy days, and even earthquakes (Mucciarelli 1998; Mucciarelli *et al.* 2003; Parolai *et al.* 2004; Parolai & Galiana-Merino 2006; Guillier *et al.* 2007; Cara *et al.* 2010). The same authors have noted that the height of the HVSR peak is less stable and not always representative of the local amplification. However, most of these observations were carried out on sites characterized by quite simple geological structures which produce a well-defined and stable resonance peak in the HVSR. On the other hand, few studies (e.g. Benkaci *et al.* 2018) have reported evidence of HVSR non-stability. In this paper we show some examples of sites where the HVSR changes significantly over time, with one or more occasional peaks appearing when the amplitude of seismic noise increases due to poor weather conditions.

2 DATA ANALYSIS AND RESULTS

The data analysed in this study were recorded at many different sites in Calabria, Italy by three-component seismic stations (Figs 1 and 2). Some of them are permanent installations of the Università della Calabria Seismic Network (www.sismocal.org), hereafter RSU (Rete Sismica Unical), while others are temporary stations installed for specific research purposes. A preliminary analysis consisted in the computation of the signal spectrum over a 600 s sliding window for continuous recordings of more than 30 seismic stations. Spectra were used to compute the power spectral density (PSD) for each component, the average PSD among the three components, and the HVSR versus time and frequency. The graphical representation of these results is very efficient for investigating the stability of HVSR in time. Weekly plotting of PSD and HVSR made it possible to identify seven sites where the HVSR shows significant variations with time that appear well correlated with the signal amplitude. Figs 3–5 show the average PSD and HVSR versus time and frequency for six sites where the variations are particularly significant. For each site, we selected two time windows in which the HVSRs show the strongest differences. The standard HVSR analysis was performed on this data selection using the software GEOPSY (www.geopsy.org), computing the spectra on a 120 s sliding window, applying an anti-triggering algorithm if necessary to remove transient disturbances, and then computing the average and standard deviation. The HVSR curves obtained from this analysis are reliable in a broad frequency range, at least from 0.1 to 30 Hz, but since we are interested in site effects in a seismic hazard perspective, we only considered the significant peaks at frequencies below 20 Hz. Since a typical feature of topographic effects is the polarization of the HVSR peak in the slope direction or perpendicular to the ridge crest (Spudich *et al.* 1996; Paolucci 2002), we also computed the HVSR as a function of azimuth using GEOPSY. Fig. 6 shows the main result of our analysis, that is, the persistent and occasional HVSR at the seven sites studied. Detailed plots for each site, showing the rms versus time, the persistent and occasional HVSR, and the HVSR versus frequency and azimuth, are shown in the Supporting Information (Supporting Information Figs S1–S7). The most relevant variations observed in the HVSRs occur during periods of higher amplitude background noise, which is strongly related to the weather conditions. Wind and sea waves can increase the amplitude of seismic noise by an order of magnitude or even more in some frequency bands. The seismic noise also shows a well-known day–night cycle associated with human activity, which is usually the main contribution at frequencies greater than 1–2 Hz (Cara *et al.* 2003; Bonnefoy-Claudet *et al.* 2006b; Koper *et al.* 2010). Hereafter we will refer to low-amplitude seismic noise during good weather periods as ‘weak noise’, and higher amplitude seismic noise recorded during periods of bad weather as ‘strong noise’. At the sites shown in Fig. 1 the HVSR exhibits one or more peaks of high amplitude that are present only during strong noise periods. Table 1 provides a summary of the main HVSR features at such sites, which are shown in Fig. 6, while RMS, HVSR versus frequency and versus azimuth are shown in the Supporting Information.

Fig. 3 shows the results of our analysis for the two sites T017 and TP02. T017 is a temporary station installed in the village of Tortora Marina, a few hundred metres from the coast (Figs 1 and 2a). Figs 3(a) and (b) respectively show the PSD and HVSR at T017 for 8 d in the 0–6 Hz frequency range. The vertical bars in the two PSD plots (a and c) mark the time periods used to compute the HVSR shown in Fig. 6a and Supporting Information Fig. S1. The HVSR computed for days of weak noise is stable with a peak of amplitude 5 at 1.4 Hz (Fig. 6a and Supporting Information Fig. S1b). On the contrary, when the signal amplitude increases, an occasional peak at 0.95 Hz shows up and increases its amplitude to reach the amplitude of the persistent peak (Fig. 6a and Supporting Information Fig. S1d). The peak around 1.4 Hz is likely associated with the resonance of a soft dipping layer. This is inferred from the higher frequency of peaks observed in HVSR at nearby sites closer to the mountain, not described here. The area around T017 is characterized by Holocene alluvial gravelly-sandy and sandy deposits. These deposits overlie the dolomitic bedrock, but the thickness of the sequence is not well defined. Fig. 6(a) also shows the results obtained for site T002, which is located less than 1 km SE of T017, in the same geological environment between the sea and the mountain, characterized by a gentle slope toward the sea (Figs 1 and 2a). The HVSR computed on weak noise shows a well-defined peak at frequency 2.1 Hz, characterized by amplitude between 4 and 5 and a wide asymmetric base that extends from 1 to 3.5 Hz, and not well-defined azimuth

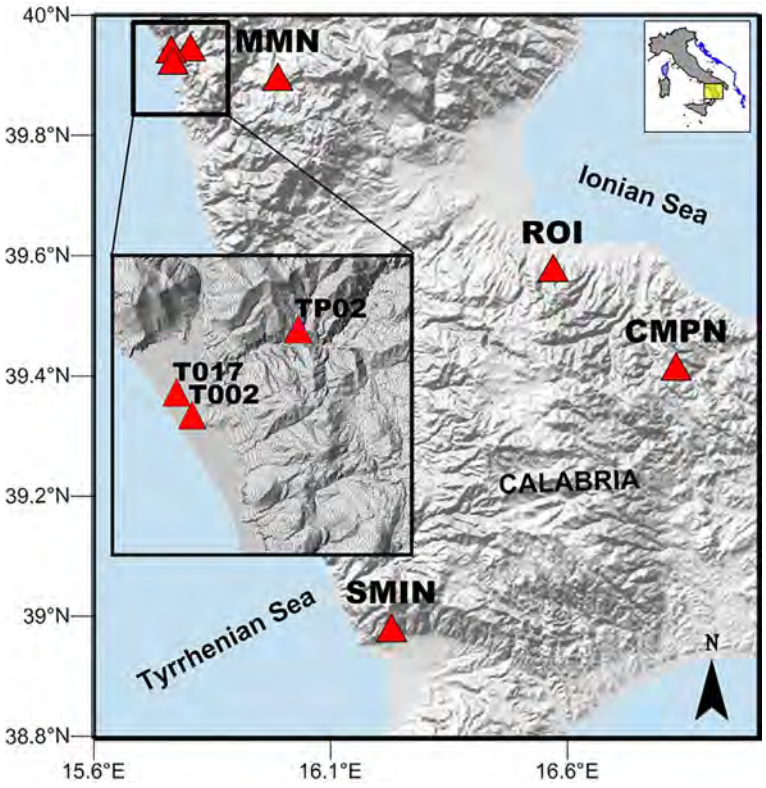

Figure 1. Topographic map showing the position of seismic stations used in this paper. MMN, ROI, CMPN and SMIN are permanent stations of the Università della Calabria Seismic Network, while T002, T017 and TP02 shown in the inset are temporary stations.

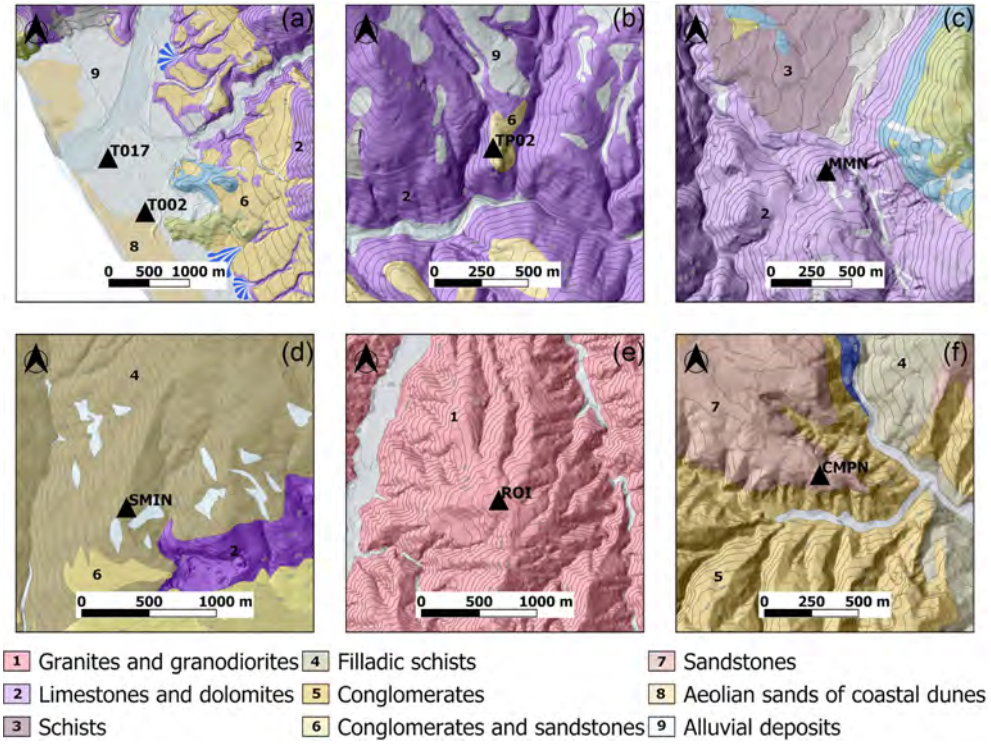

Figure 2. Topographic and geological maps of the area surrounding the seven sites analysed in this paper.

(Fig. 6a, and Supporting Information Figs S2b and c). In the case of strong noise, the peak at 2.1 Hz increases its amplitude up to 8, and a second peak rises at 1.3 Hz with an azimuth of 45° (Supporting Information Figs S2d and e). The case of T002 is qualitatively very similar to T017, but both persistent and occasional peaks occur at higher frequency.

Figs 3(c) and (d) show the results of data recorded at site TP02 (Figs 1 and 2b) by a temporary station installed in the basement of a

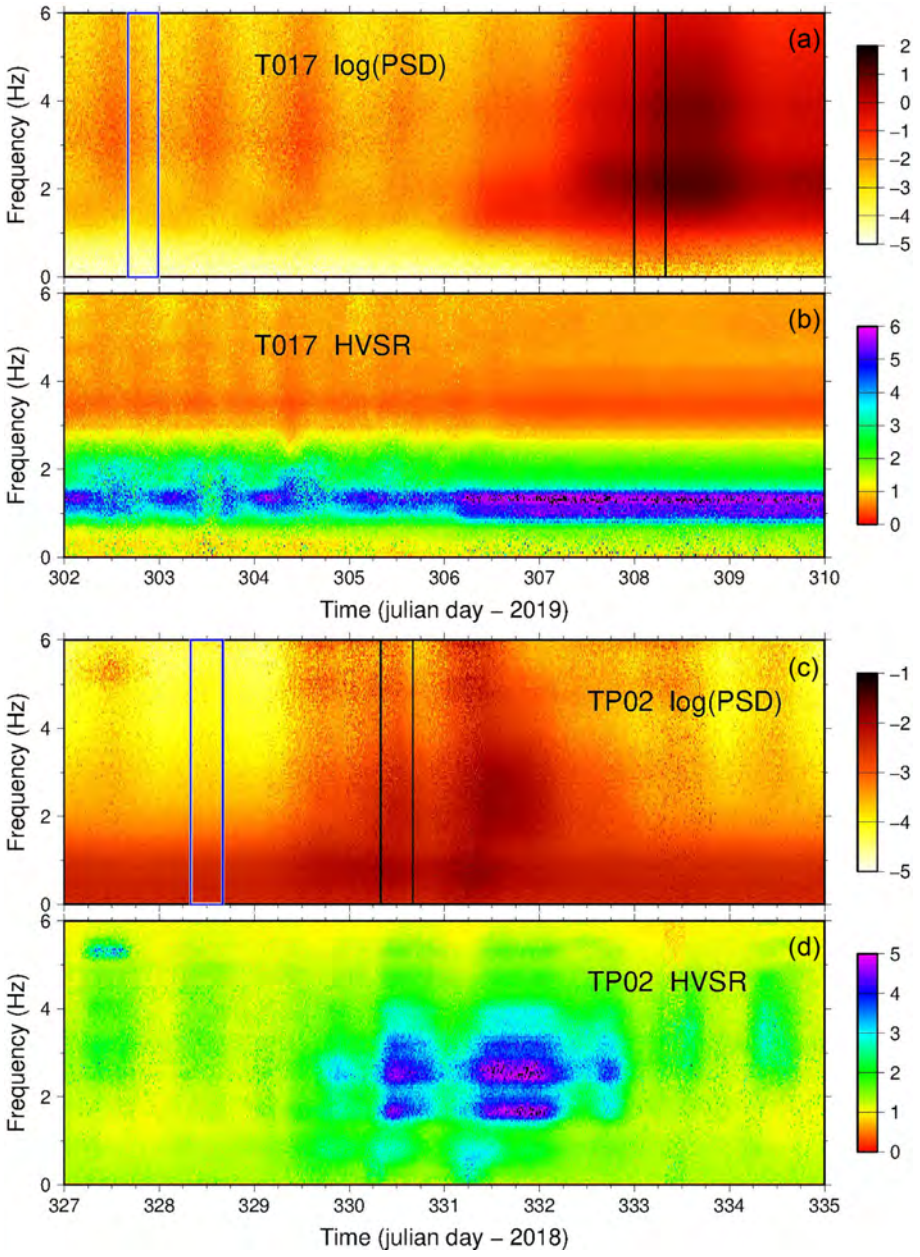

Figure 3. Logarithm of PSD (mean among the three components of ground motion, reference is 1 micron^2 s^{-2}) and HVSR versus time and frequency at stations T017 (plots a and b) and TP02 (plots c and d) for 8 d of data. The blue and black boxes in the PSD plot show the 8-hr time window used to compute the HVSR plotted in Fig. 6.

church in the historical centre of the village Tortora, at the southern end of a small ridge oriented north–south. The geology is characterized by a few metres of Pliocene sands and conglomerates that overlie the well-bedded dolomitic bedrock (Triassic in age) through an unconformity surface. At TP02 the weak noise HVSR is flat in a broad frequency band (Fig. 6b, and Supporting Information Figs S3b and c), without any peaks which satisfy the significance criteria established by the Sesame project (Sesame 2004). This result was expected because the area is characterized by outcropping bedrock. Only a peak at about 15 Hz is very stable, but its average amplitude is just below 2, while some peaks between 2 and 5 Hz perturb the flat average value occasionally. On the contrary, in the case of strong noise the HVSR is very different, with two peaks at 1.6 and 2.6 Hz, amplitude greater than 4, and a well-defined azimuth of about 80° (Figs 3d and 6b, and Supporting Information Figs S3d and e). The frequencies of these peaks and their E–W polarization suggest that their origin could be a topographic amplification of the horizontal ground motion in the direction normal to the N-S oriented crest (Fig. 2).

Fig. 4 shows the results of data recorded at sites MMN and SMIN. MMN is a permanent station of the RSU installed in a vault of the cemetery of the village Mormanno (Figs 1 and 2c). The area around this site is characterized by complex topography with a ravine nearby to the north and the irregular outcropping of well-bedded dolomitic rocks, often intensely fractured. A formation of calc-schist rock is present very close northwards. The weak noise HVSR is characterized by an irregular increase of amplitude with frequency, with a pair of stable peaks between 5 Hz and 7 Hz, and

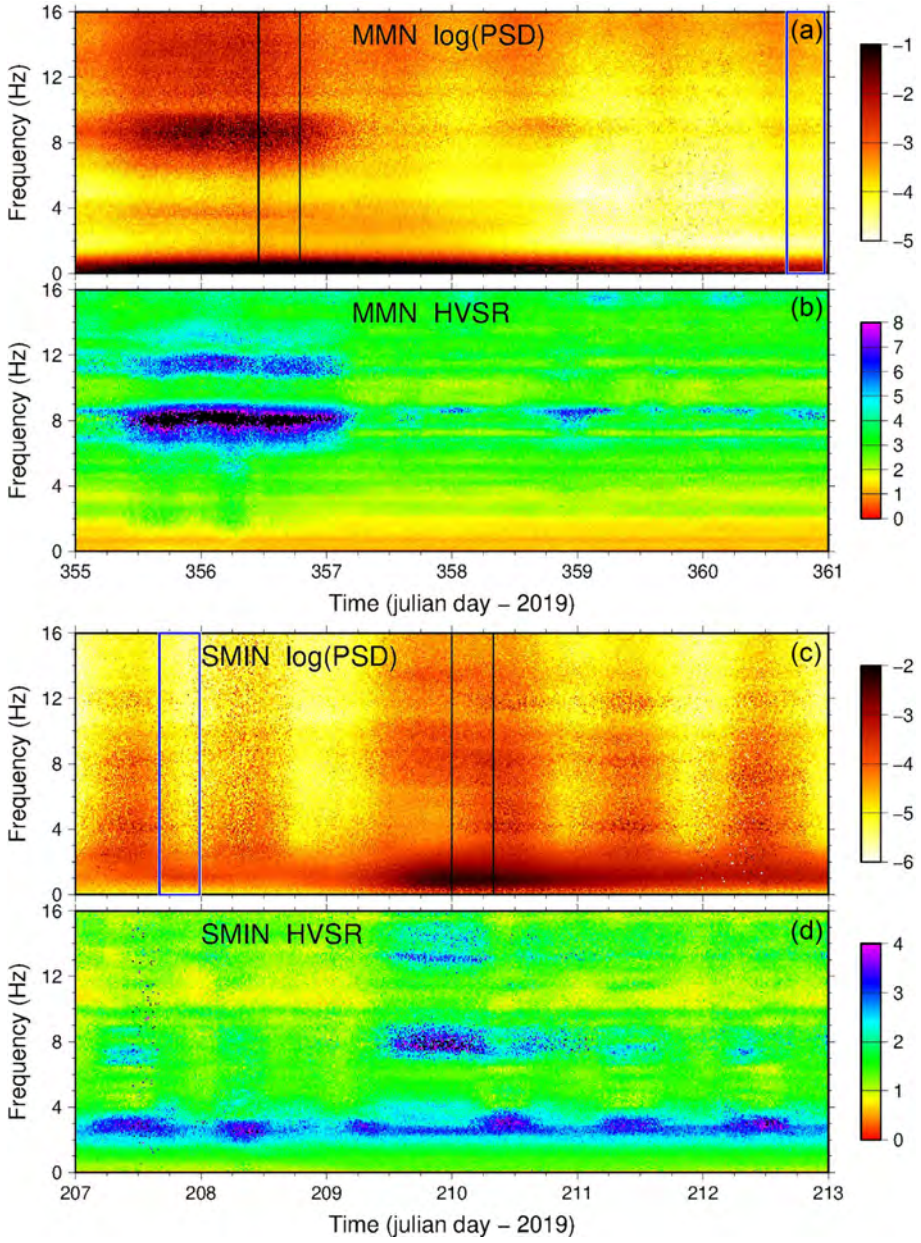

Figure 4. Logarithm of PSD and HVSR versus time and frequency at stations MMN (plots a and b) and SMIN (plots c and d) for 6 d of data.

another broad peak between 11 and 20 Hz (Figs 4b and 6c and Supporting Information Fig. S4b). In the case of strong noise the HVSR contains two well-defined significant peaks at 7.6 and 11 Hz (Figs 4b and 6c and Supporting Information Fig. S4d). These peaks reach an H/V value greater than 8 and 6, respectively, and both are polarized in the N–S direction (Supporting Information Fig. S4e). The direction of maximum slope at the MMN site is N–S (Fig. 2c), thus the polarization of the two occasional peaks could be related to topographic effects.

SMIN is a permanent station of the RSU installed inside an abandoned house on a hill slope (Figs 1 and 2d). A formation of filladic schist (Palaeozoic) rich in chlorite, sericite and quartz outcrop widely around SMIN. Southeastwards, the tectonic contact between this formation and the Triassic dolomites also occurs. The weak noise HVSR is quite stable, characterized by a broad peak of amplitude up to 3 at frequency 2.5 Hz (Figs 4d and 6d and Supporting Information Fig. S5b). In the case of strong noise the HVSR remains the same up to 6 Hz, while it changes a great deal at higher frequency, where two peaks at 8 and 14 Hz increase their amplitude up to 3 and 2.5, respectively (Figs 4d and 6d and Supporting Information Fig. S5d). The polarization of the occasional peaks at 8 and 14 Hz is the same (140°), but it is completely different compared with the persistent peak at 2.5 Hz (about 80°). At the site SMIN an amplitude modulation of the persistent weak noise HVSR correlated with the day–night cycle is evident.

Fig. 5 shows the results of the analysis of seismic data recorded at sites ROI and CMPN. ROI is a permanent station of the RSU installed on an N–S oriented ridge (Figs 1 and 2e). The area around ROI is dominated by a complex of intrusive Palaeozoic acidic rocks (diorite, quartz monzonite, granodiorite and granite) often deeply weathered and tectonized. The weak noise HVSR is characterized by irregular shape with a broad double peak of amplitude 3 between 6 and 10 Hz (Figs 5b and 6e and Supporting Information Fig. S6b). In the strong noise HVSR the double peak

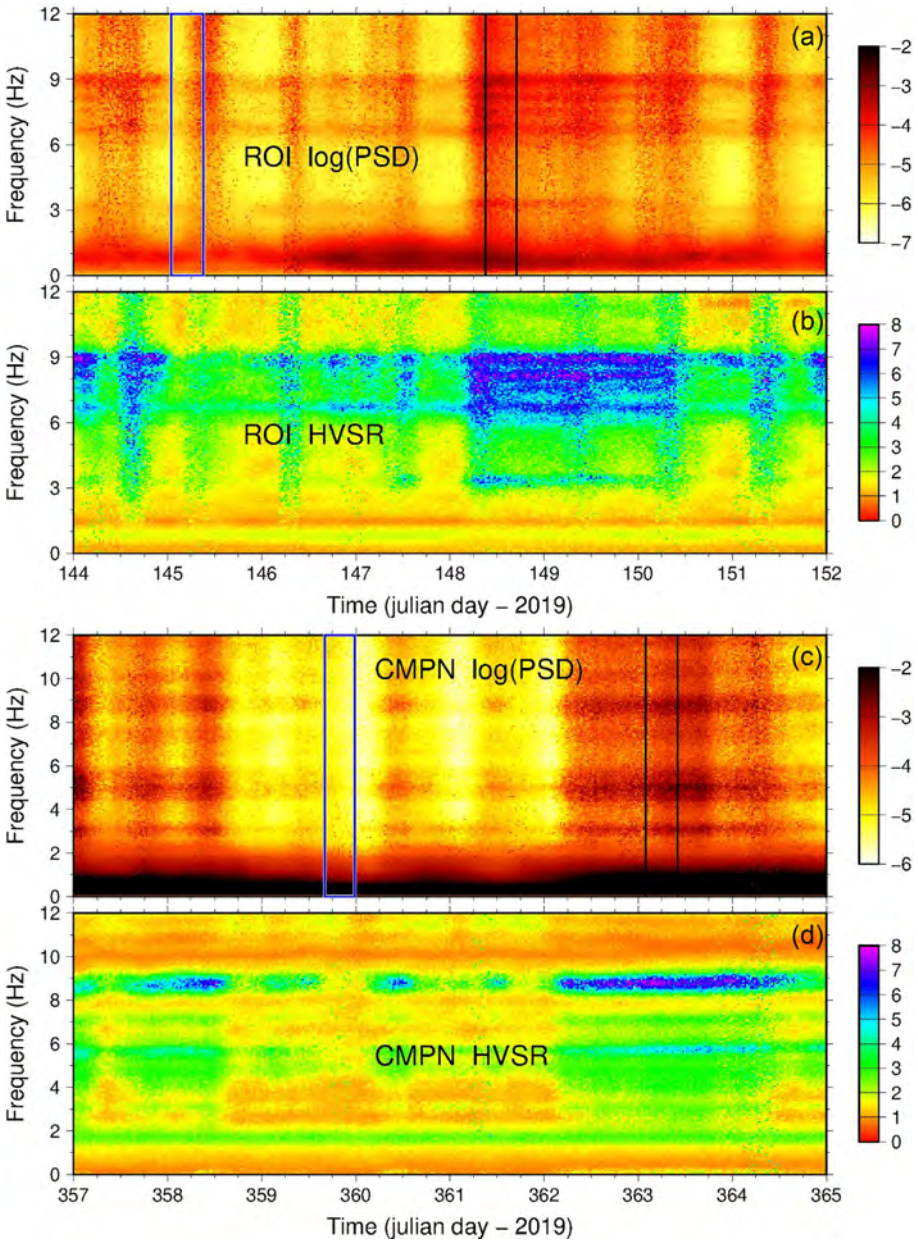

Figure 5. Logarithm of PSD and HVSR versus time and frequency at stations ROI (plots a and b) and CMPN (plots c and d) for 8 d of data.

between 6 and 10 Hz increases its amplitude up to 7, and another well-defined peak at frequency 3.3 Hz appears with amplitude up to 5. It is interesting to note the completely different polarization of the peaks that characterize the strong noise: 160° for the broad peak between 6 and 10 Hz versus 60° for the occasional peak at 3.3 Hz. An amplitude modulation of the persistent weak noise HVSR correlated with the day–night cycle is evident at the site ROI.

CMPN is a permanent station of the RSU installed in the crypt of a medieval church in the historical centre of the village Campana (Figs 1 and 2f). The old part of the village around this church is built upon a ridge oriented WNW–ESE (Fig. 2f), and all the houses in a radius of 150 m are abandoned, therefore no artificial sources of noise are usually present very near the instrument. Campana is built above a Miocenic sedimentary sequence, a formation of well-consolidated sandstones overlying well-bedded conglomerate rocks. The weak noise HVSR has only one significant peak of amplitude 3 at 1.6 Hz (Figs 5d and 6f, and Supporting Information Fig. S7b). On the contrary, the strong noise HVSR shows a high narrow peak at 9 Hz, and another peak of lower amplitude at 5.5 Hz (Figs 5d and 6f, and Supporting Information Fig. S7d). The persistent peak at 1.6 Hz is very stable in shape, frequency and amplitude, with an azimuth polarization of about 40°. This is the direction perpendicular to the ridge crest, therefore this occasional peak is very likely produced by a topography effect. The high occasional peak at 9 Hz has the same well-defined polarization, while the peak at 5.5 Hz seems less polarized (Supporting Information Fig. S7e).

Fig. 6 shows a summary of the results described above and depicted in Figs 3–5, and in the Supporting lnformation (Supporting Information Figs S1–S7). For each site, the weak noise (persistent, red line) and strong noise (occasional, blue line) HVSRs are shown. The shadowed area represents one standard deviation above and below the mean value. It is noteworthy that the amplitude of the strong

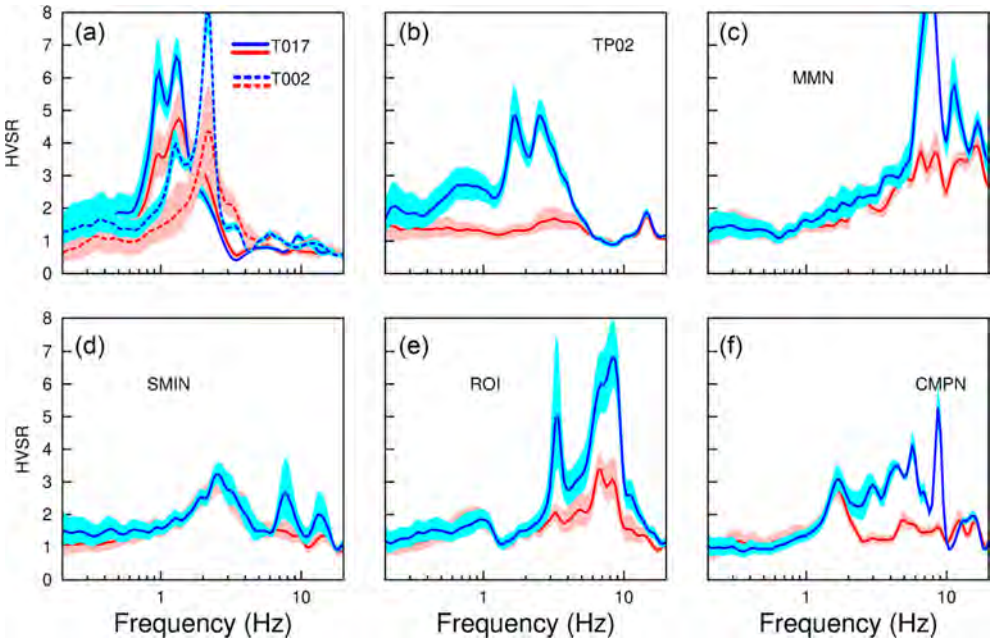

Figure 6. Mean values of persistent (red line) and occasional (blue line) HVSR at the seven sites studied in this paper. These results are obtained from the analysis of 8 hr of signals, as shown by blue and black boxes in Figs 3–5. Shadowed area represents one standard deviation above and below the mean. HVSRs shown here were computed by GEOPSY over 120 s sliding window, taking the square average of horizontal component spectra over the vertical component spectrum.

Table 1. Persistent and occasional HVSR peaks.

Site	Persistent peak			Occasional peak		
	Freq (Hz)	Amp	Azimuth	Freq (Hz)	Amp	Azimuth
T017	1.4	5	120° ± 20°	0.95	6.5	40° ± 20°
T002	2.15	4	–	1.3	4	45° ± 15°
TP02	15	1.8	60° ± 20°	1.7	4.8	80° ± 20°
				2.6	4.8	80° ± 20°
MMN	6.5	4	0° ± 20°	7.6	>8	170° ± 20°
	8.5	3.7	0° ± 20°	11	6	170° ± 20°
	17	4	0° ± 20°			
SMIN	2.5	3	90° ± 20°	8	2.8	140° ± 20°
				14	2.2	140° ± 20°
ROI	7	3.3	160° ± 30°	3.3	5	60° ± 20°
	8.5	3	160° ± 30°			
CMPN	1.6	3	40° ± 20°	5.5	4	90° ± 20°
				9	5	40° ± 20°

noise HVSR curve is always greater than or equal to the weak noise curve.

3 DISCUSSION

We have described seven sites where the HVSR is characterized by dual contents, one persistent contribution that is typical of weak noise, and another contribution that appears when the amplitude of seismic noise increases. These sites are geologically different from each other and are not located on flat land. All of them have HVSRs with at least one significant persistent peak, which may be representative of a soft layer resonance or of topographic effects. The two sites near the coast, T002 and T017, are located on almost flat land, but it is a narrow belt between the sea and the mountain (Figs 1 and 2a). At these two sites the weak noise HVSR shows a well-defined peak corresponding to the resonance of a soft layer that is dipping toward the sea. The other five sites (TP02, MMN, ROI, CMPN, SMIN) are all located on hill slopes or on a ridge crest, in places where the soft soil on bedrock is negligible or very thin. At these sites it is difficult to interpret the HVSR obtained from weak noise because we expect contributions from both the geology and topography (Burjanek *et al.* 2014), and they are not easily discernible from each other. The occasional peaks that rise when the signal amplitude is higher have a completely different frequency among the analysed sites, from 0.9 Hz at T017 to 14 Hz at SMIN (Table 1). This wide range in frequency corresponds to a wide range in wavelength. For example, assuming Vs = 1 km s^{-1} in the weathered, highly fractured bedrock near the surface, the corresponding wavelength ranges from 70 m to 1 km. Therefore the size of structures likely involved in the generation of the occasional HVSR peaks spans from less than 100 m to an entire mountain.

The sites at Tortora Marina, T002 and T017, located in between the sea and the mountain, show a well-defined, persistent high peak

that testify the resonance of a sedimentary layer along the coast. A survey of seismic noise measurements carried out in the area of Tortora Marina, not described in this paper, shows that the frequency of the HVSR peak increases with increasing distance from the shoreline. This result indicates a decreasing depth of the bedrock going toward the mountain, where it is outcropping and HVSRs are quite flat. From this observation we infer that the thickness of the soft surface layer along the coast increases westward. The occasional peak that appears at lower frequency in the case of strong noise does not fit with the rather simple model of one soft dipping layer on the bedrock. A possible explanation of this result is the effect of a shear head wave produced by the sea waves as they approach the coast. The HVSR peak associated with shear head waves has been theoretically described by Bonnefoy-Claudet *et al.* (2006a). Unfortunately, our single-station data are not sufficient to confirm or reject this hypothesis.

Three sites are located on a ridge crest (TP02, ROI, CMPN), where a significantly competent bedrock is outcropping or covered by only a few metres of soft soil. The weak noise HVSRs of these sites are characterized by peaks of small amplitude that likely correspond to topographic effects. The remaining two analysed sites are located on hill slopes in a mountain environment (MMN and SMIN). For all the five sites in the mountains the occasional contribution to the HVSR yields peaks at frequencies greater than T002 and T017, from 1.7 up to 14 Hz. The persistent HVSR peaks at the seven studied sites all show a polarization in the horizontal plane (see Table 1 and Supporting Information Fig. S8 for a summary). Those attributed to the topography have polarizations parallel to the slope direction (MMN, SMIN) or normal to the ridge crest (TP02, ROI, CMPN), while those corresponding to layer resonance are polarized in the same direction to the presumed layer dipping (T002, T017).

It is not easy to establish why strong noise changes the HVSR at these sites. All analysed data were acquired by seismic stations installed inside a building (house basement, cellar, vault, and similar locations) with the seismometer covered by a shelter and thermally insulated in the case of a broad band sensor, therefore the direct action of wind, rain, and any other perturbing phenomena upon the instruments can be excluded. We have taken the possibility that occasional peaks may be produced by the resonance of some buildings or other artificial structures nearby the recording sites into account, but could not find anything likely responsible for the occasional peaks. We also checked for wind generators but could not find any in a radius of many km from each studied site. Our hypothesis is that strong noise has a different wavefield composition compared with weak noise, thus the interaction with the local structure and with the topography produces different effects than those observed during weak noise periods. It is impossible to establish the composition of the background seismic wavefield from single-station data and we do not have appropriate array data for a full characterization of the seismic wavefield. The contribution of surface and body waves in the background signal is variable, being dependent on the noise sources, their features and distance from the recording site. The boundary at about 1 Hz that separate microseismic natural signal from artificial source noise is also quite variable and site dependent (Bonnefoy-Claudet *et al.* 2006b; Guillier *et al.* 2007). On the other hand, an increasing contribution of body waves in the background seismic noise as the frequency increases has been documented (Koper *et al.* 2010). The hypothesis that strong noise has greater body wave content than weak noise well supports the occasional low-frequency peak that shows up in the HVSR at the two sites near the coast, T002 and T017, as inferred by some theoretical analyses (Bonnefoy-Claudet *et al.* 2006a). The interaction of body waves with local topography could also explain the occasional peaks observed at the other sites described here. In fact we find a good correlation between the polarization of occasional HVSR peaks and the direction of maximum slope or the direction normal to the ridge crest (Supporting Information Fig. S8). The important contribution of body waves to topographic effects has been recognized in many studies (Geli *et al.* 1988; Sanchez-Sesma & Campillo 1993; Chavez-Garcia *et al.* 1996, 1997). Assuming that at frequencies greater than 1 Hz, strong noise contains a greater amount of body waves compared with weak noise, the hypothesis that occasional peaks seen in the strong noise HVSR are produced by the interaction of body waves with topography and geological structure is very likely. This hypothesis is also consistent with the amplitude modulation of the HVSR peak correlated with the day–night cycle at some of the studied sites.

The last point to be discussed is the possible influence of fault zones near the investigated site. It is known that fault zones modify the propagation of seismic waves, producing amplification and polarization of the ground motion (e.g. Rigano *et al.* 2008; Pischiutta *et al.* 2012). This could be the origin of some occasional peaks seen in the strong noise HVSR. However, at present our knowledge of the size and position of fault zones in the areas around the seven sites studied in this paper is not sufficient to attempt any investigations in this direction.

Looking at the results shown in Figs 3–5, a variation of the HVSR amplitude following the day–night cycle is recognized at many stations during the weak noise periods. Although the HVSR shape is quite stable, the height of the main peak increases during the day, when the background noise has higher amplitude, and decreases during the night hours. The reason is likely the same that gives rise to the occasional peaks in the case of strong noise, but at present we do not have an exhaustive explanation. In fact, the variations of the background wavefield contents between day and night hours is a complex topic that can only be investigated with dense arrays. At frequencies greater than 1 Hz, some authors have observed increasing contents of body waves during day hours attributed to human activity (e.g. Koper *et al.* 2010), while in some other cases the body waves seem predominant during night hours (e.g. Peruzzetto *et al.* 2018).

4 CONCLUSIONS

The study described in this paper demonstrates that in some cases the HVSR result is not stable in time and its interpretation is far from obvious. While in the past decades many papers have shown the stability of HVSR at sites characterized by a rather simple geological structure, our results indicate that this is not necessarily true at sites characterized by rough topography and/or complex geological structure. In such cases the results of HVSR analyses may be different depending on the amplitude, and likely other features, of the incoming waves. The HVSR amplitude of strong noise is always greater than or equal to the HVSR of weak noise at each studied site (Fig. 6). This means that in the case of strong noise, the horizontal ground motion is amplified more than the vertical motion at the frequencies of occasional peaks. The well-defined polarization of most occasional peaks suggests a key role played by the topography. Our results pose an important limitation to the interpretation of HVSR in places where a combination of different site effects may occur. However, more observations are necessary to reach a satisfying comprehension of the occasional HVSR peaks. First of all, good knowledge of the geological structure at the investigated

site and in the surrounding area is necessary, including a 3-D velocity model. Recordings of the seismic wavefield by three-component seismic arrays could give important insights on the properties of the seismic waves whose interaction with the local geological structure gives rise to occasional HVSR peaks. Another important point is the investigation of possible fault zones nearby the site that show variable HVSR peaks.

The results described in this paper suggest paying much more attention to the interpretation of HVSR in all cases where the topography around the investigated site is not negligible and the local geological structure is not simple. In such cases, analysing only an hour of signal recordings may give misleading results.

ACKNOWLEDGEMENTS

Comments by Herve Chauris and an anonymous reviewer greatly improved the paper quality.

REFERENCES

Benkaci, N., Oubaiche, E.H., Chatelain, J., Bensalem, R., Benouar, D. & Abbes, K., 2018. Non-stability and non-reproducibility of ambient vibration HVSR peaks in Algiers (Algeria), *J. Earthq. Eng.,* 1–19, doi:10.1080/13632469.2018.153790.

Bignardi, S., 2017. The uncertainty of estimating the thickness of soft sediments with the HVSR method: a computational point of view on weak lateral variations, *J. Appl. Geophys.,* **145,** 28–38.

Bonnefoy-Claudet, S., Cornou, C., Bard, P.Y., Cotton, F., Moczo, P., Kristek, J. & Fäh, D., 2006a. H/V ratio: a tool for site effects evaluation. Results from 1-D noise simulations, *Geophys. J. Int.,* **167**(2), 827–837.

Bonnefoy-Claudet, S., Cotton, F. & Bard, P.Y., 2006b. The nature of noise wavefield and its applications for site effects studies. A literature review, *Earth Sci. Rev.,* **79**(3-4), 205–227.

Bonnefoy-Claudet, S., Köhler, A., Cornou, C., Wathelet, M. & Bard, P.Y., 2008. Effects of love waves on microtremor H/V ratio, *Bull. seism. Soc. Am.,* **98**(1), 288–300.

Borges, J.F., Silva, H.G., Torres, R.J.G., Caldeira, B., Bezzeghoud, M., Furtado, J.A. & Carvalho, J., 2016. Inversion of ambient seismic noise HVSR to evaluate velocity and structural models of the Lower Tagus Basin, Portugal, *J. Seismol.,* **20**(3), 875–887.

Bouchon, M. & Barker, J.S., 1996. Seismic response of a hill: the example of Tarzana, California, *Bull. seism. Soc. Am.,* **86**(1A), 66–72.

Bour, M., Fouissac, D., Dominique, P. & Martin, C., 1998. On the use of microtremor recordings in seismic Microzonation, *Soil Dyn. Earthq. Eng.,* **17,** 465–474.

Buech, F., Davies, T.R. & Pettinga, J.R., 2010. The Little Red Hill seismic experimental study: topographic effects on ground motion at a bedrock-dominated mountain edifice, *Bull. seism. Soc. Am.,* **100**(5A), 2219–2229.

Burjanek, J., Edwards, B. & Fah, D., 2014. Empirical evidence of local seismic effects at sites with pronounced topography: a systematic approach, *Geophys. J. Int.,* **197,** 608–619.

Cara, F., Di Giulio, G. & Rovelli, A., 2003. A study on seismic noise variations at Colfiorito, central Italy: implications for the use of H/V spectral ratios, *Geophys. Res. Lett.,* **30**(18), 1972, doi:10.1029/2003GL017807.

Cara, F., Di Giulio, G., Milana, G., Bordoni, P., Haines, J. & Rovelli, A., 2010. On the stability and reproducibility of the horizontal-to-vertical spectral ratios on ambient noise: case study of Cavola, Northern Italy, *Bull. seism. Soc. Am.,* **100**(3), 1263–1275.

Chavez-Garcia, F.J., Sanchez, L.R. & Hatzfeld, D., 1996. Topographic site effects and HVSR. A comparison between observations and theory, *Bull. seism. Soc. Am.,* **86**(5), 1559–1573.

Chavez-Garcia, F.J., Rodriguez, M., Field, E.H. & Hatzfeld, D., 1997. Topographic site effects. A comparison of two nonreference methods, *Bull. seism. Soc. Am.,* **87**(6), 1667–1673.

Chavez-Garcia, F.J., Monsalve, H., Gomez-Cano, M. & Vila Ortega, J.J., 2018. Vulnerability and site effects in earthquake disasters in Armenia (Colombia). I—Site Effects, *Geosciences,* **8,** 254, doi:10.3390/geosciences8070254.

Del Gaudio, V., Coccia, S., Wasowski, J., Gallipoli, M.R. & Mucciarelli, M., 2008. Detection of directivity in seismic site response from microtremor spectral analysis, *Nat. Hazards Earth Syst. Sci.,* **8,** 751–762.

Formisano, L.A., La Rocca, M., Del Pezzo, E., Galluzzo, D., Fischione, C. & Scarpa, R., 2012. Topography effects in the polarization of earthquake signals: a comparison between surface and deep recordings, *Boll. Geofis. Teor. Appl.,* **53**(4), 471–484.

Gallipoli, M.R., Albarello, D., Mucciarelli, M. & Bianca, M., 2011. Ambient noise measurements to support emergency seismic microzonation: the Abruzzo 2009 earthquake experience, *Boll. Geofis. Teor. Appl.,* **52,** 539–559.

Geli, L., Bard, P.Y. & Jullien, B., 1988. The effect of topography on earthquake ground motion: A review and new results, *Bull. seism. Soc. Am.,* **78**(1), 42–63.

Gosar, A. & Lenart, A., 2010. Mapping the thickness of sediments in the Ljubljana Moor basin (Slovenia) using microtremors, *Bull. Earthq. Eng.,* **8,** 501–518.

Gueguen, P., Chatelain, J.-L., Guillier, B., Yepes, H. & Egred, J., 2000. An indication of the soil topmost layer response in Quito (Ecuador) using noise H/V spectral ratio, *Soil Dyn. Earthq. Eng.,* **19,** 127–133.

Guillier, B., Chatelain, J.-L., Bonnefoy-Claudet, S. & Haghshenas, E., 2007. Use of ambient noise: from spectral amplitude variability to H/V stability, *J. Earthq. Eng.,* **11**(6), 925–942.

Koper, K.D., Seats, K. & Benz, H., 2010. On the composition of earth's Short-Period seismic noise field, *Bull. seism. Soc. Am.,* **100**(2), 606–617.

Lachet, D., Hatzfeld, C., Bard, P.Y., Theodulis, N., Papaioannou, C. & Savvaidis, A., 1996. Site effects and microzonation in the city of Thessaloniki (Greece), comparison of different approaches, *Bull. seism. Soc. Am.,* **86,** 1692–1703.

Lermo, J. & Chavez-Garcia, F.J., 1993. Site effect evaluation using spectral ratios with only one station, *Bull. seism. Soc. Am.,* **83,** 1574–1594.

Martorana, R., Capizzi, P., D'Alessandro, A., Luzio, D., Di Stefano, P., Renda, P. & Zarcone, G., 2018. Contribution of HVSR measures for seismic microzonation studies, *Ann. Geophys.,* **61**(2), SE225, doi:10.441/ag-7786.

Massa, M., Lovati, S., D'Alema, E., Ferretti, G. & Bakavoli, M., 2010. An experimental approach for estimating seismic amplification effects at the top of a ridge, and the implication for ground-motion predictions: the case of Narni, Central Italy, *Bull. seism. Soc. Am.,* **100**(6), 3020–3034.

Mucciarelli, M., 1998. Reliability and applicability of Nakamura's technique using microtremors: an experimental approach, *J. Earthq. Eng.,* **2,** 625–638.

Mucciarelli, M., 2011. Ambient noise measurements following the 2011 Christchurch earthquake: relationships with previous microzonation studies, liquefaction, and nonlinearity, *Seismol. Res. Lett,* **82**(6), 919–926.

Mucciarelli, M. & Gallipoli, M.R., 2001. A critical review of 10 years of microtremor HVSR technique, *Boll. Geofis. Teor. Appl.,* **42**(3–4), 255–266.

Mucciarelli, M., Gallipoli, M.R. & Arcieri, M., 2003. The stability of the Horizontal-to-Vertical spectral ratio of triggered noise and earthquake recordings, *Bull. seism. Soc. Am.,* **93**(3), 1407–1412.

Nakamura, Y., 1989. A method for dynamic characteristics estimations of subsurface using microtremors on the ground surface, *Q. Rep. Railw. Tech. Res. Inst. Japan,* **30,** 25–33.

Nakamura, Y., 2000. Clear identification of fundamental idea of Nakamura's technique and its applications, in *Proc. 12th World Conf. on Earthq. Eng.,* Auckland, New Zealand, 8pp.

Napolitano, F., Gervasi, A., La Rocca, M., Guerra, I. & Scarpa, R., 2018. Site effects in the Pollino region from spectral and polarization analyses of seismic noise and earthquakes, *Bull. seism. Soc. Am.,* **108,** 309–321.

Panzera, F., Lombardo, G. & Rigano, R., 2011. Evidence of topographic effects through the analysis of ambient noise measurements, *Seismol. Res. Lett.,* **82,** 413–419.

Paolucci, R., 2002. Amplification of earthquake ground motion by steep topographic irregularities, *Earthq. Eng. Struct. Dyn.,* **31,** 1831–1853.

Parolai, S. & Galiana-Merino, J.J., 2006. Effect of Transient Seismic Noise on Estimates of H/V Spectral Ratios, *Bull. seism. Soc. Am,* **96**(1), 228–236.

Parolai, S., Bormann, P. & Milkereit, C., 2002. New Relationships between Vs, Thickness of Sediments, and Resonance Frequency Calculated by the H/V Ratio of Seismic Noise for the Cologne Area (Germany), *Bull. seism. Soc. Am.,* **92**(6), 2521–2527.

Parolai, S., Richwalski, S.M., Milkereit, C. & Bormann, P., 2004. Assessment of the stability of H/V spectral ratios from ambient noise and comparison with earthquake data in the Cologne area (Germany), *Tectonophysics* **390**(1), 57–73.

Parolai, S. *et al.*, 2010. Site effects assessment in Bishkek (Kyrgyzstan) using earthquake and noise recording data, *Bull. seism. Soc. Am.,* **100**(6), 3068–3082.

Pedersen, H., Le Brun, B., Hatzfeld, D., Campillo, M. & Bard, P.Y., 1994. Ground motion amplitude across ridges, *Bull. Seism. Soc. Am,* **84**(6), 1786–1800.

Peruzzetto, M., Kazantsev, A., Luu, K., Metaxian, J.P., Huguet, F. & Chauris, H., 2018. Broad-band ambient noise characterization by joint use of cross-correlation and MUSIC algorithm, *Geophys. J. Int.,* **215,** 760–779.

Pischiutta, M., Salvini, F., Fletcher, J., Rovelli, A. & Ben-Zion, Y., 2012. Horizontal polarization of ground motion in the Hayward fault zone at Fremont, California: dominant fault-high-angle polarization and fault-induced cracks, *Geophys. J. Int.,* **188**(3), 1255–1272.

Rigano, R., Cara, F., Lombardo, G. & Rovelli, A., 2008. Evidence for ground motion polarization on fault zones of Mount Etna volcano, *J. geophys. Res.,* **113,** B10306, doi:10.1029/2007JB005574.

Rong, M., Fu, L.-Y., Wang, Z., Li, X., Carpenter, N.S., Woolery, E.W. & Lyu, Y., 2017. On the amplitude discrepancy of HVSR and site amplification from strong-motion observations, *Bull. seism. Soc. Am.,* **107**(6), 2873–2884.

Sanchez-Sesma, F.J. & Campillo, M., 1993. Topographic effects for incident P, SV and Rayleigh waves, *Tectonophysics,* **218,** 113–125.

SESAME WP12 team, 2004. Guidelines for the implementation of the H/V spectral ratio technique on ambient vibrations-measurements, processing and interpretation. SESAME European research project WP12 -Deliverable D23.12.

Spudich, P., Hellweg, M. & Lee, W.H.K., 1996. Directional topographic site response at Tarzana observed in aftershocks of the 1994 Northridge, California, earthquake: implications for mainshock motions, *Bull. seism. Soc. Am.,* **86**(1B), S193–S208.

Strollo, A., Parolai, S., Bindi, D., Chiauzzi, L., Pagliuca, R., Mucciarelli, M. & Zschau, J., 2012. Microzonation of Potenza (Southern Italy) in terms of spectral intensity ratio using joint analysis of earthquakes and ambient noise, *Bull. Earthq. Eng.,* **10**(2), 493–516.

SUPPORTING INFORMATION

Supplementary data are available at *GJI* online.

Figure S1. Results of the seismic noise analysis at T017. Plot (a) shows the rms computed for 8 d of signals bandpass filtered in two different frequency bands: 0.7–2 Hz (red line) and 0.7–1.2 Hz (blue line). Rms were computed on a 600 s sliding window for the three components, then the mean value was computed. Plots (b) and (c) show the plain and directional H/V spectral ratio of weak signal computed in the 8 hr time window shown by background colour in plot (a). Plots (d) and (e) show the plain and directional HVSR of strong signal. The dashed box in plots (c) and (e) marks the polarization azimuth of HVSR peak.

Figure S2. Results of the analyses at the site T002. Plot (a) shows the rms computed for 10 d of signals bandpass filtered in two different frequency bands: 1.4–3 Hz (red line) and 0.8–1.5 Hz (blue line). Plots (b) and (c) show the plain and directional H/V spectral ratio of weak signal computed in the 8 hr time window shown by background colour in plot (a). Plots (d) and (e) show the plain and directional HVSR of strong signal. The dashed box in plot (e) marks the polarization azimuth of occasional HVSR peak.

Figure S3. Results of the analysis of seismic noise at site TP02. Plot (a) shows the rms computed for 6 d of signals bandpass filtered in the frequency band 1.3–4 Hz. Plots (b) and (c) show the plain and directional H/V spectral ratio of weak signal computed in the 8 hr time window shown by background color in plot (a). Plots (d) and (e) show the plain and directional HVSR of strong signal. The dashed box in plots (c) and (e) marks the polarization azimuth of HVSR peak.

Figure S4. Results of the analysis of seismic noise at site MMN. Plot (a) shows the rms computed for 7 d of signals bandpass filtered in two different frequency bands: 0.2–2 Hz (red line) and 6–14 Hz (blue line). Plots (b) and (c) show the plain and directional H/V spectral ratio of weak signal computed in the 8 hr time window shown by background color in plot (a). Plots (d) and (e) show the plain and directional HVSR of strong signal. The dashed box in plots (c) and (e) marks the polarization azimuth of HVSR peak.

Figure S5. Results of the analysis of seismic noise at site SMIN. Plot (a) shows the rms computed for 6 d of signals bandpass filtered in two different frequency bands: 0.2–2 Hz (red line) and 7–17 Hz (blue line). Plots (b) and (c) show the plain and directional H/V spectral ratio of weak signal computed in the 8 hr time window shown by background colour in plot (a). Plots (d) and (e) show the plain and directional HVSR of strong signal. The dashed box in plots (c) and (e) marks the polarization azimuth of HVSR peak.

Figure S6. Results of the analysis of seismic noise at site ROI. Plot (a) shows the rms computed for 8 d of signals bandpass filtered in three different frequency bands: 0.2–2 Hz (red line), 2.2–4.5 Hz (magenta line) and 6–10 Hz (blue line). Plots (b) and (c) show the plain and directional H/V spectral ratio of weak signal computed in the 8 hr time window shown by background color in plot (a). Plots (d) and (e) show the plain and directional HVSR of strong signal. The dashed box in plots (c) and (e) marks the polarization azimuth of HVSR peak.

Figure S7. Results of the analysis of seismic noise at site CMPN. Plot (a) shows the rms computed for 10 d of signals bandpass filtered in three different frequency bands: 0.2–2 Hz (red line), 4–8 Hz (blue line) and 8–10 Hz (magenta line). Plots (b) and (c) show the plain and directional H/V spectral ratio of weak signal computed in the 8 hr time window shown by background color in plot (a). Plots (d) and (e) show the plain and directional HVSR of strong signal. The dashed boxes in plots (c) and (e) mark the polarization azimuth of HVSR peaks.

Figure S8. Polarization of the occasional HVSR peaks versus the direction normal to ridge crest (a) and versus the direction of maximum slope (b).

Please note: Oxford University Press is not responsible for the content or functionality of any supporting materials supplied by the authors. Any queries (other than missing material) should be directed to the corresponding author for the paper.

Non-stability of the noise HVSR at sites near or on topographic heights

M. La Rocca[(1)], G. D. Chiappetta[(1)], A. Gervasi[(2,1)], R. L. Festa[(1)]

Supplementary material.

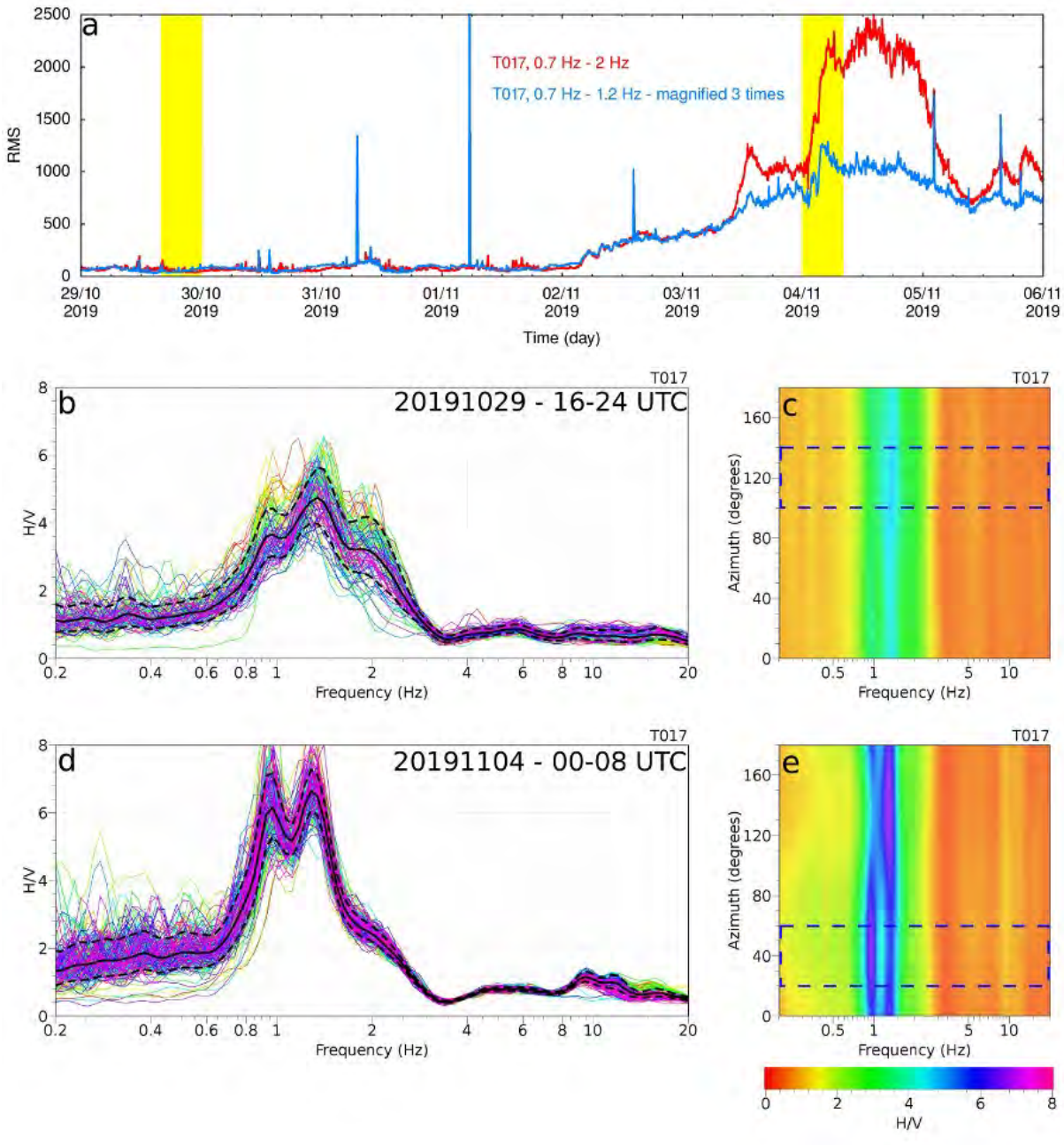

Figure S1. Results of the seismic noise analysis at T017. Plot a shows the rms computed for 8 days of signals bandpass filtered in two different frequency bands: 0.7 – 2 Hz (red line) and 0.7 – 1.2 Hz (blue line). Rms were computed on a 600 s sliding window for the three components, then the mean value was computed. Plots b and c show the plain and directional H/V spectral ratio of weak signal computed in the 8 hours time window shown by background color in plot a. Plots d and e show the plain and directional HVSR of strong signal. The dashed box in plots c and e marks the polarization azimuth of HVSR peak.

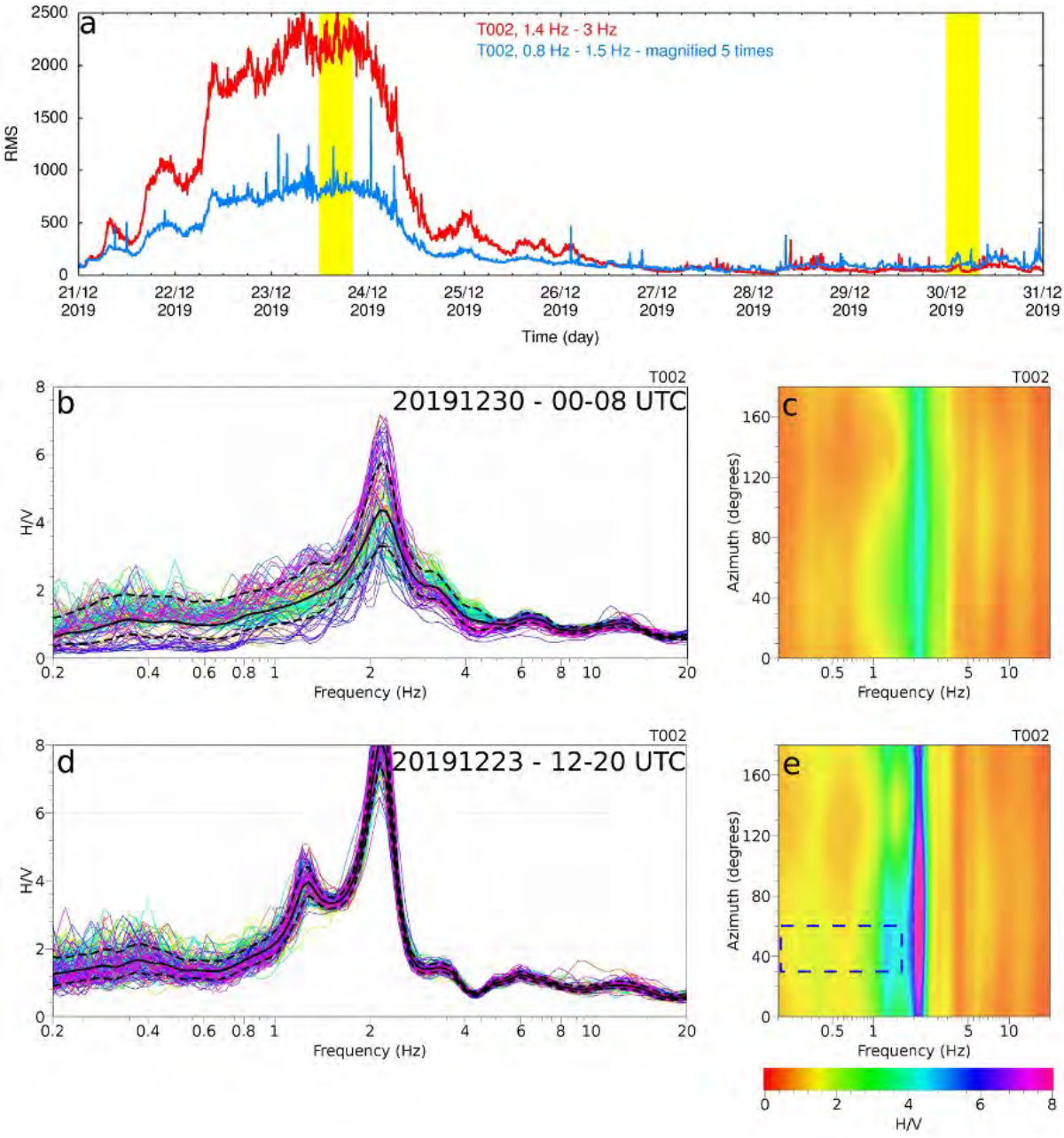

Figure S2. Results of the analyses at the site T002. Plot a shows the rms computed for 10 days of signals bandpass filtered in two different frequency bands: 1.4 – 3 Hz (red line) and 0.8 – 1.5 Hz (blue line). Plots b and c show the plain and directional H/V spectral ratio of weak signal computed in the 8 hours time window shown by background color in plot a. Plots d and e show the plain and directional HVSR of strong signal. The dashed box in plot e marks the polarization azimuth of occasional HVSR peak.

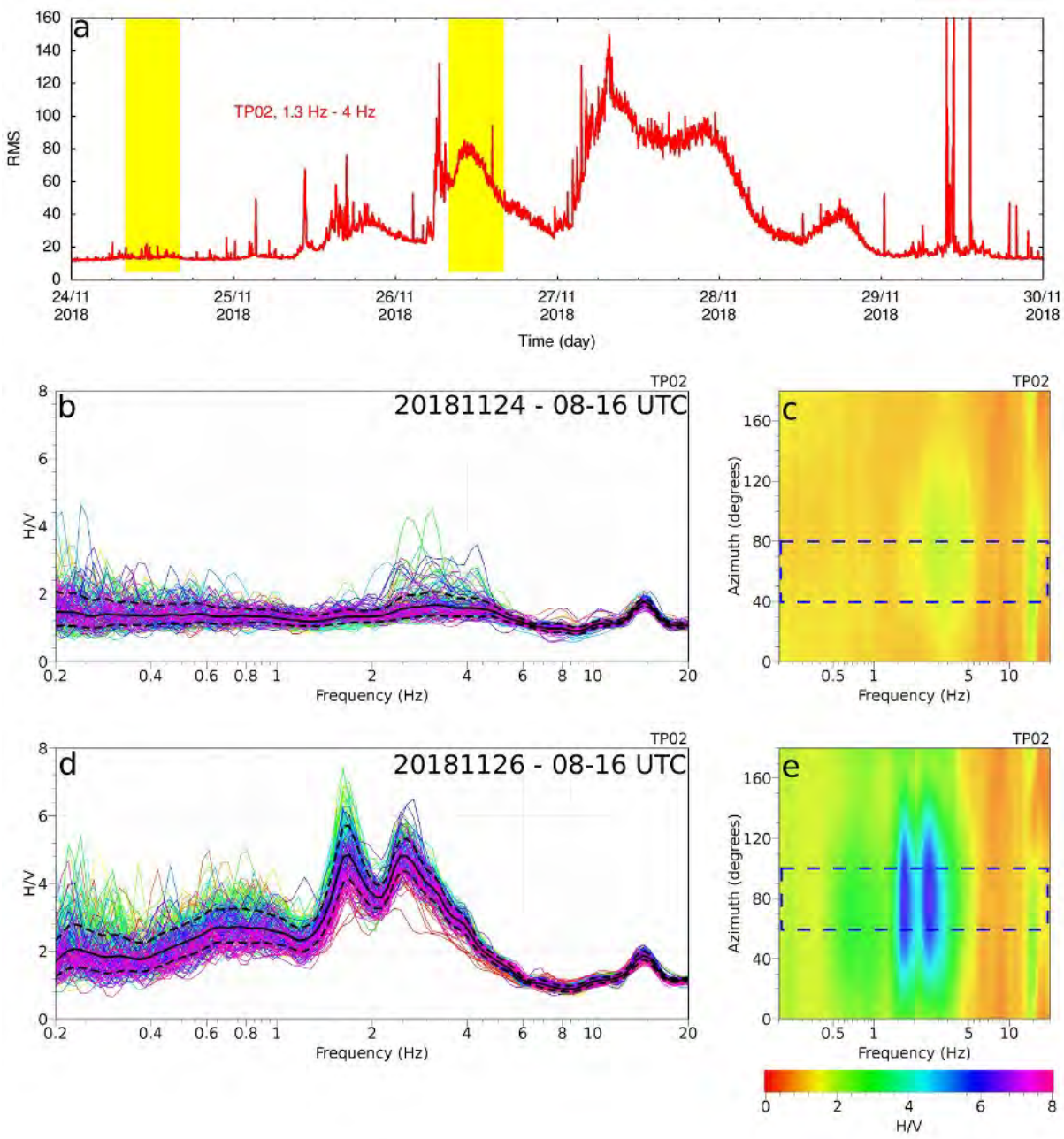

Figure S3. Results of the analysis of seismic noise at site TP02. Plot a shows the rms computed for 6 days of signals bandpass filtered in the frequency band 1.3 – 4 Hz. Plots b and c show the plain and directional H/V spectral ratio of weak signal computed in the 8 hours time window shown by background color in plot a. Plots d and e show the plain and directional HVSR of strong signal. The dashed box in plots c and e marks the polarization azimuth of HVSR peak.

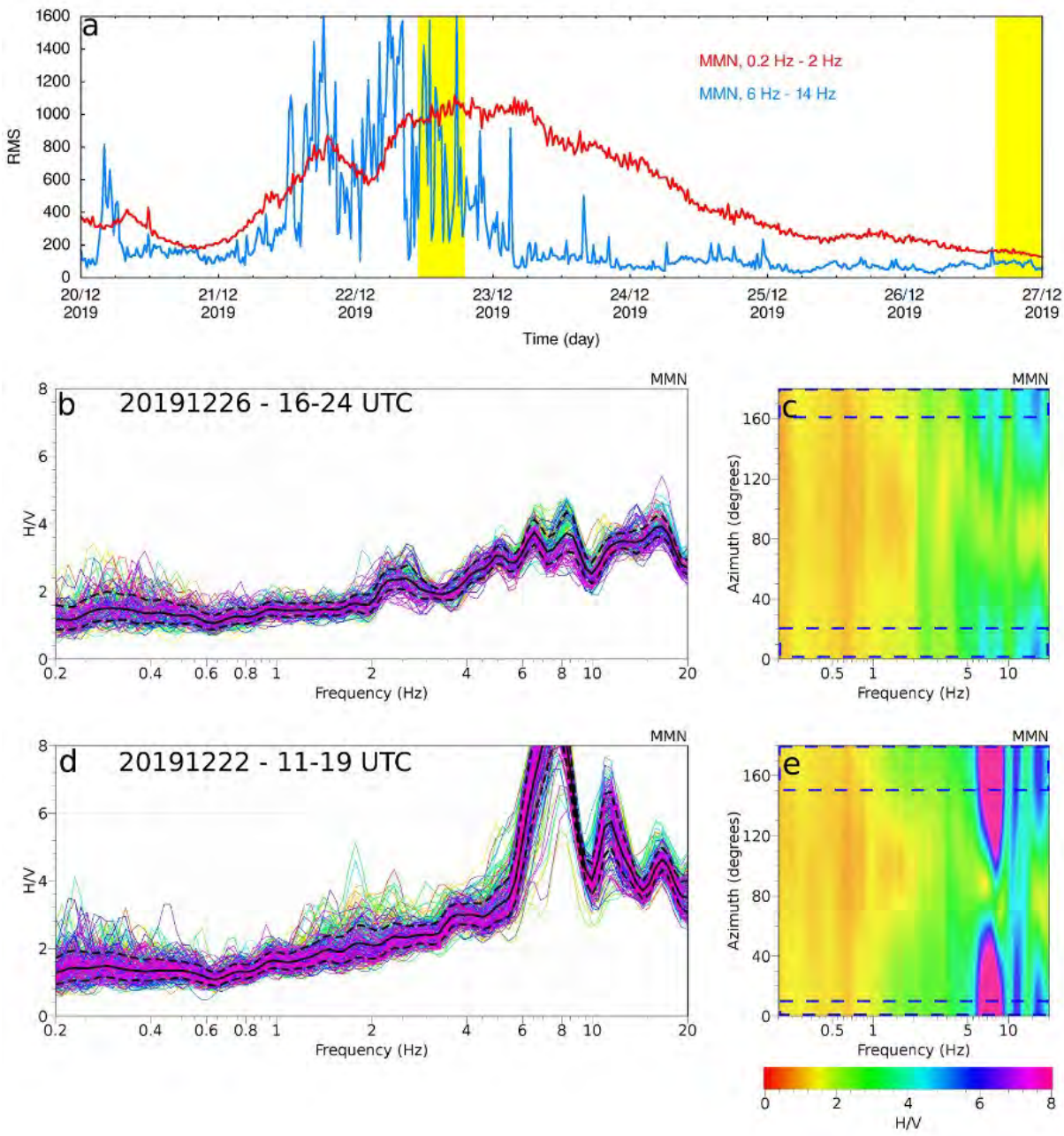

Figure S4. Results of the analysis of seismic noise at site MMN. Plot a shows the rms computed for 8 days of signals bandpass filtered in two different frequency bands: 0.2 – 2 Hz (red line) and 6 – 14 Hz (blue line). Plots b and c show the plain and directional H/V spectral ratio of weak signal computed in the 8 hours time window shown by background color in plot a. Plots d and e show the plain and directional HVSR of strong signal. The dashed box in plots c and e marks the polarization azimuth of HVSR peak.

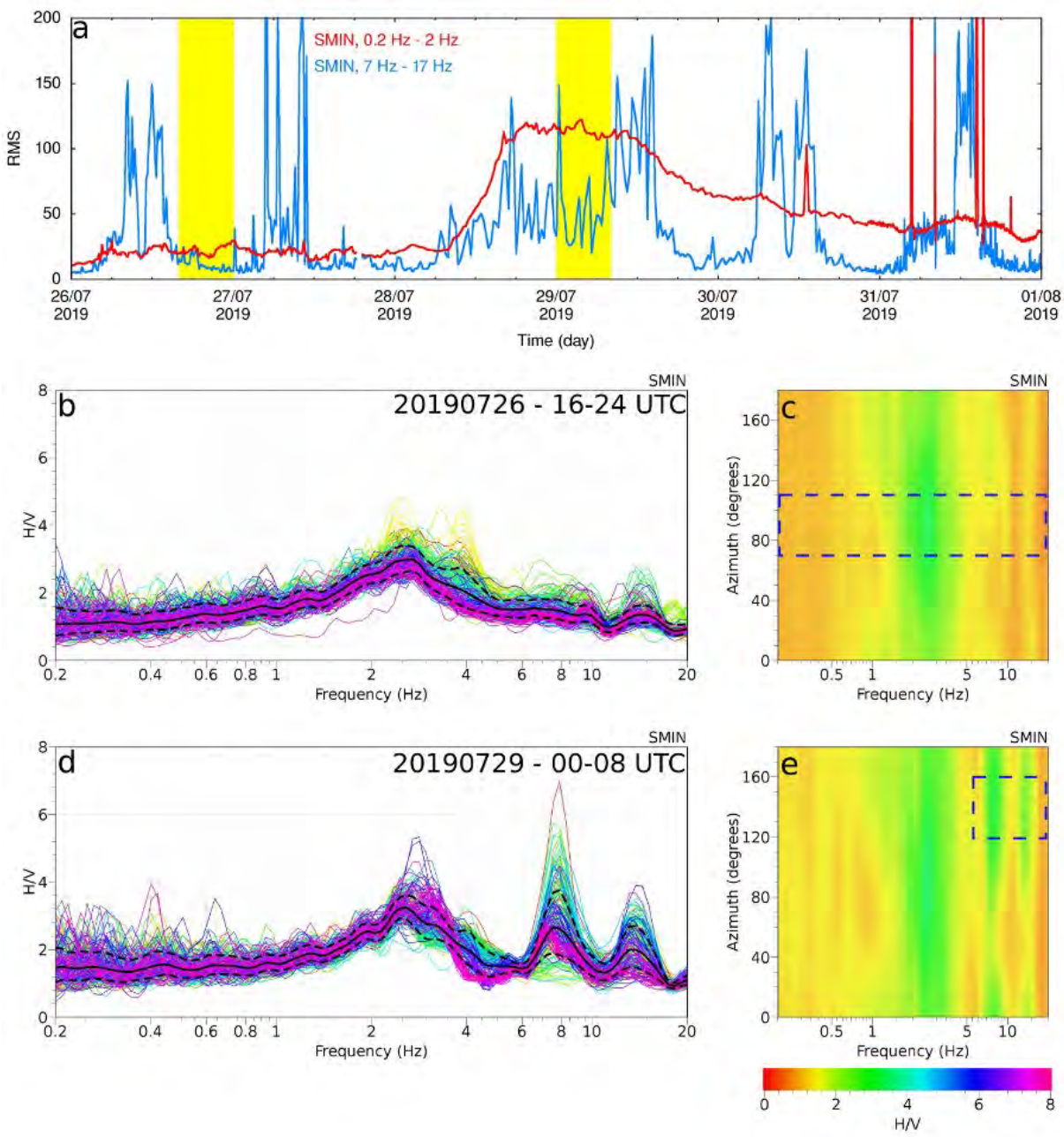

Figure S5. Results of the analysis of seismic noise at site SMIN. Plot a shows the rms computed for 6 days of signals bandpass filtered in two different frequency bands: 0.2 – 2 Hz (red line) and 7 – 17 Hz (blue line). Plots b and c show the plain and directional H/V spectral ratio of weak signal computed in the 8 hours time window shown by background color in plot a. Plots d and e show the plain and directional HVSR of strong signal. The dashed box in plots c and e marks the polarization azimuth of HVSR peak.

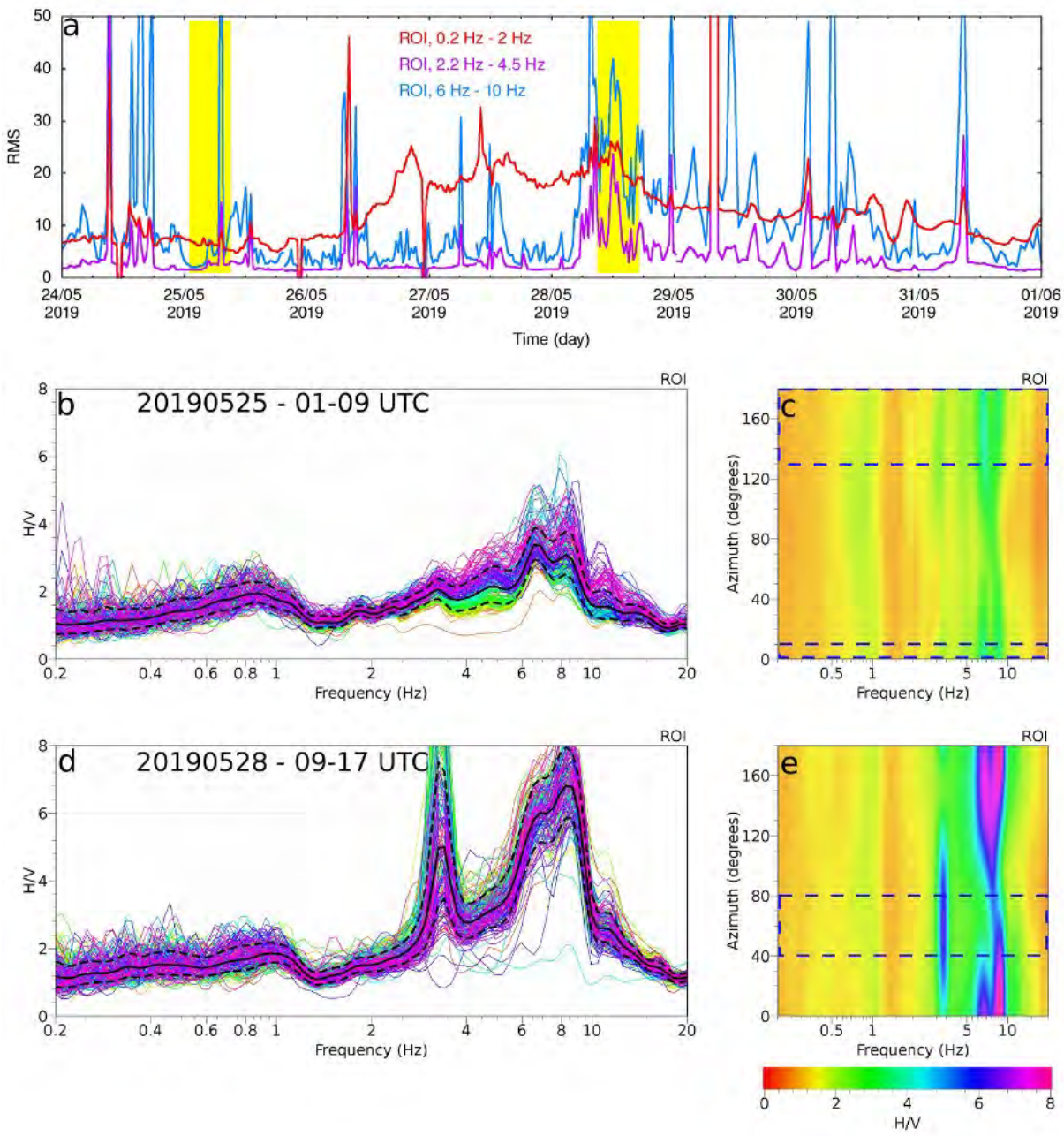

Figure S6. Results of the analysis of seismic noise at site ROI. Plot a shows the rms computed for 8 days of signals bandpass filtered in three different frequency bands: 0.2 – 2 Hz (red line), 2.2 – 4.5 Hz (magenta line) and 6 – 10 Hz (blue line). Plots b and c show the plain and directional H/V spectral ratio of weak signal computed in the 8 hours time window shown by background color in plot a. Plots d and e show the plain and directional HVSR of strong signal. The dashed box in plots c and e marks the polarization azimuth of HVSR peak.

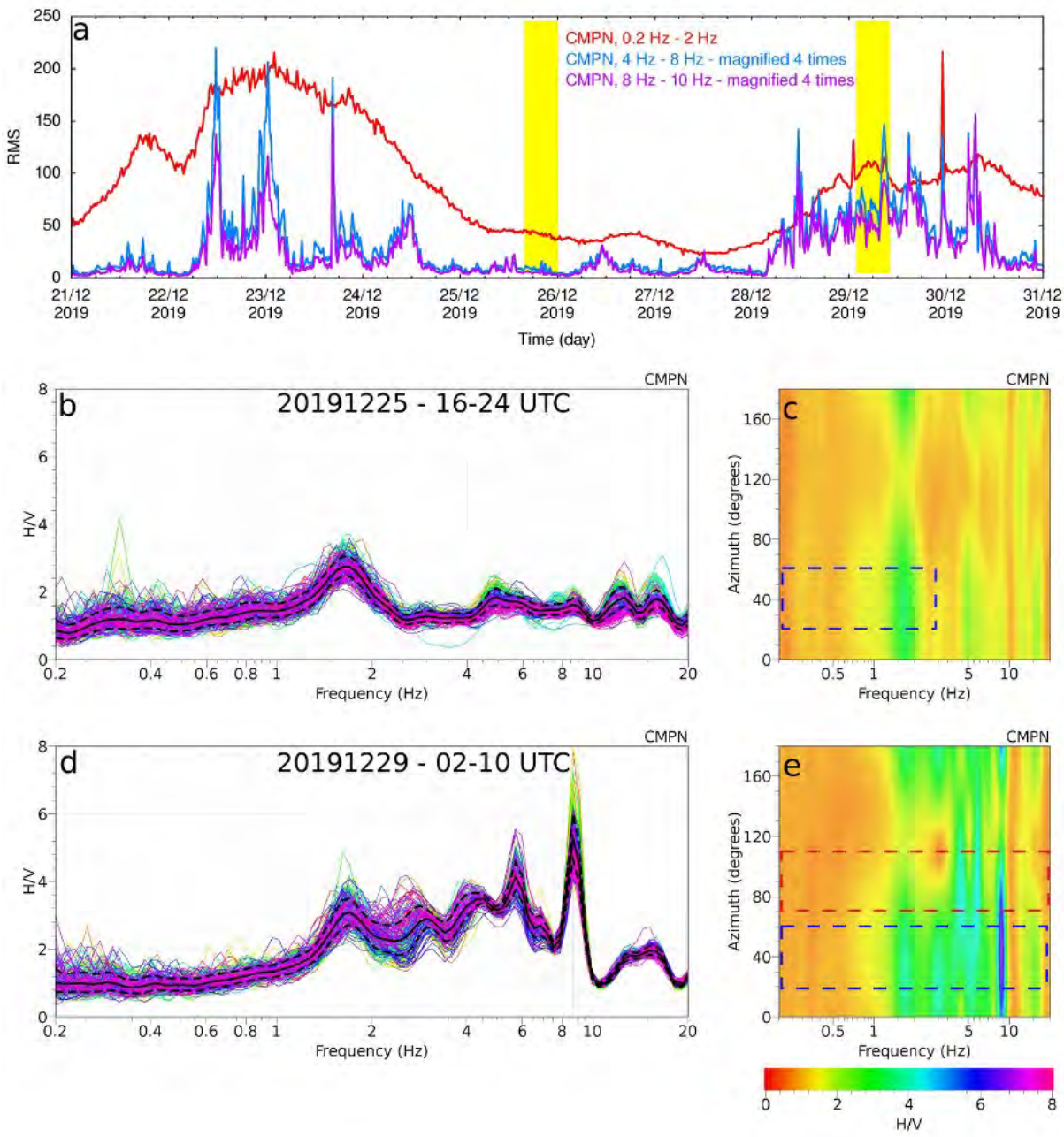

Figure S7. Results of the analysis of seismic noise at site CMPN. Plot a shows the rms computed for 8 days of signals bandpass filtered in three different frequency bands: 0.2 – 2 Hz (red line), 4 – 8 Hz (blue line) and 8 – 10 Hz (magenta line). Plots b and c show the plain and directional H/V spectral ratio of weak signal computed in the 8 hours time window shown by background color in plot a. Plots d and e show the plain and directional HVSR of strong signal. The dashed boxes in plots c and e mark the polarization azimuth of HVSR peaks.

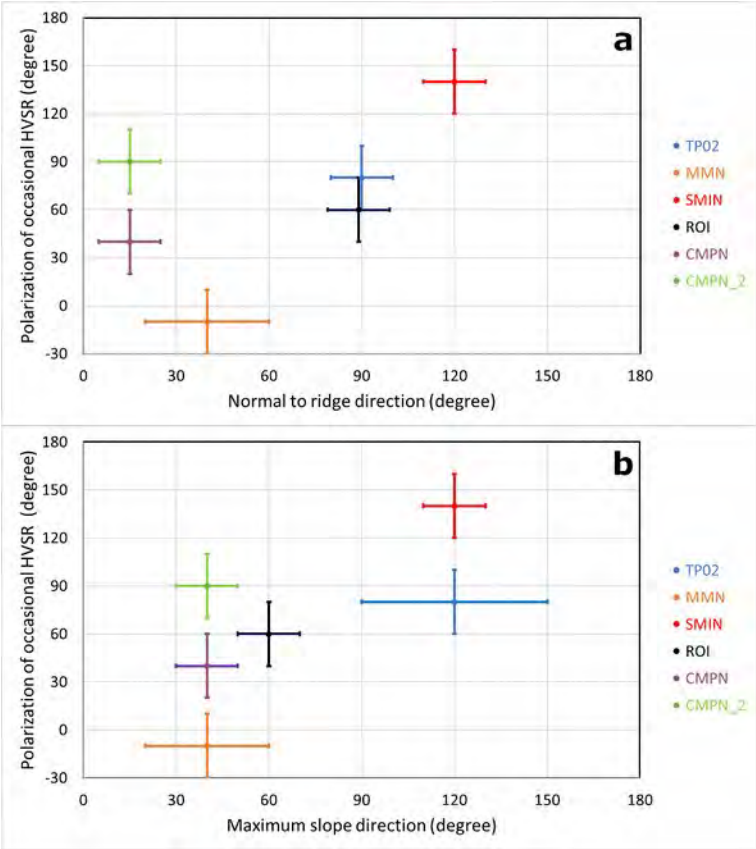

Figure S8. Polarization of the occasional HVSR peaks versus the direction normal to ridge crest (a) and versus the direction of maximum slope (b).